iScience, Volume *23*

Supplemental Information

Cellular and Molecular Changes of Brain Metastases-Associated Myeloid Cells during Disease Progression and Therapeutic Response

Michael Schulz, Birgitta Michels, Katja Niesel, Stefan Stein, Henner Farin, Franz Rödel, and Lisa Sevenich

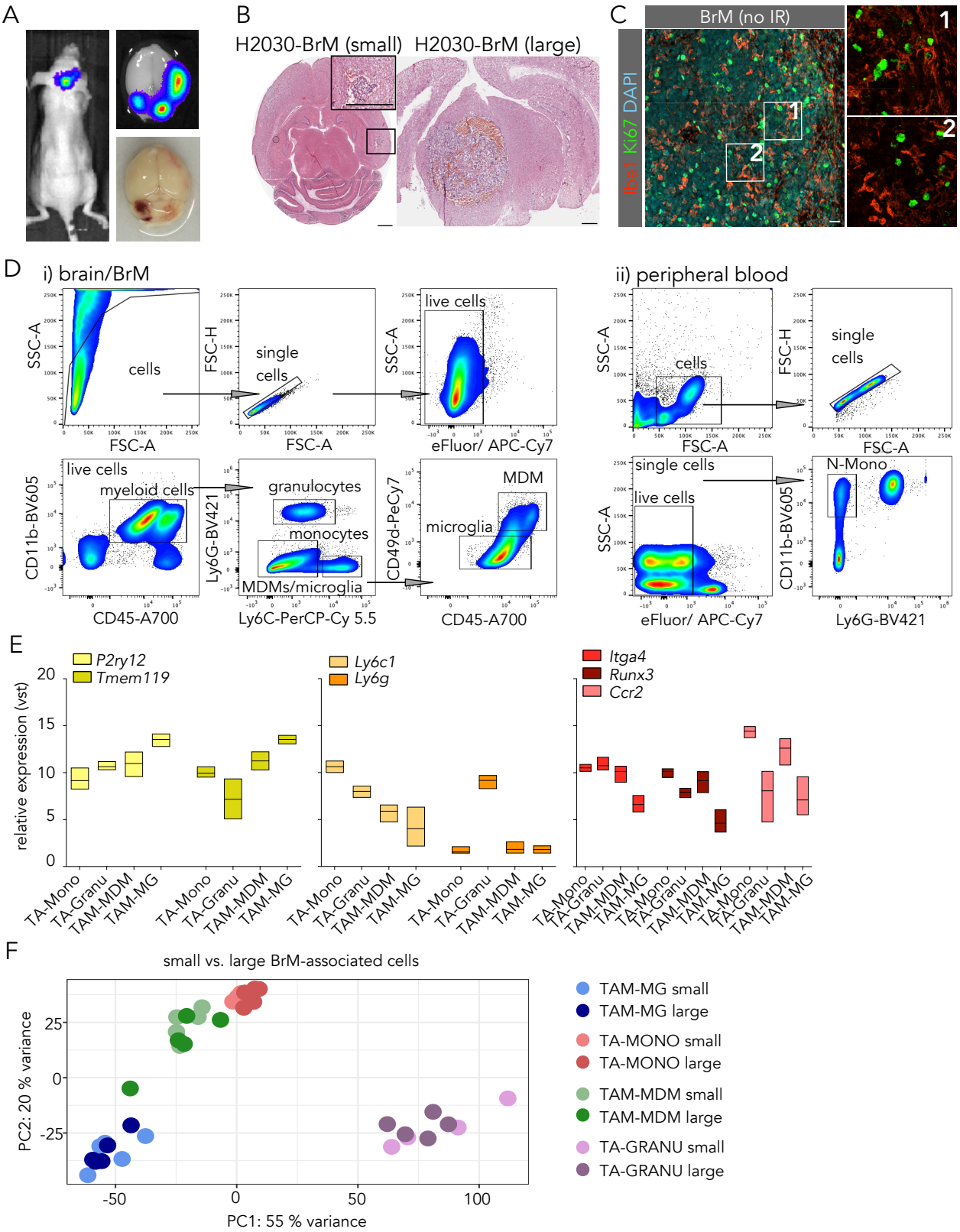

Figure S1. Analysis of the TME in H2030-BrM, related to Figure 1. **(A)** Macroscopic images of BLI signal of a representative H2030-BrM bearing mouse and the corresponding photograph of the brain. **(B)** H&E stainings of brain sections with small (left) or large (right) H2030-BrMs. Scale bar depicts 1 mm. **(C)** Representative immunofluorescence image of proliferating cells within and adjacent to H2030-BrM lesions. Sections were stained for Iba1 to visualize microglia/macrophages (red) and the proliferation marker Ki67 (green). Scale bar; 50 µm. **(D)** Representative gating strategy for flow cytometry and cell sorting for (BrM-bearing) brain (i) and blood monocytes (N-Mono) isolated from peripheral blood (ii). **(E)** Quantification of RNA-Seq data showing expression levels of distinct cell-type specific genes to validate the purity of sorted cell populations. **(F)** PCA plot of BrM-associated cells in small vs. large BrM. TA = tumor-associated. n=4 for TA-Mono and TA-Granu from small BrM and n=5 for all other groups.

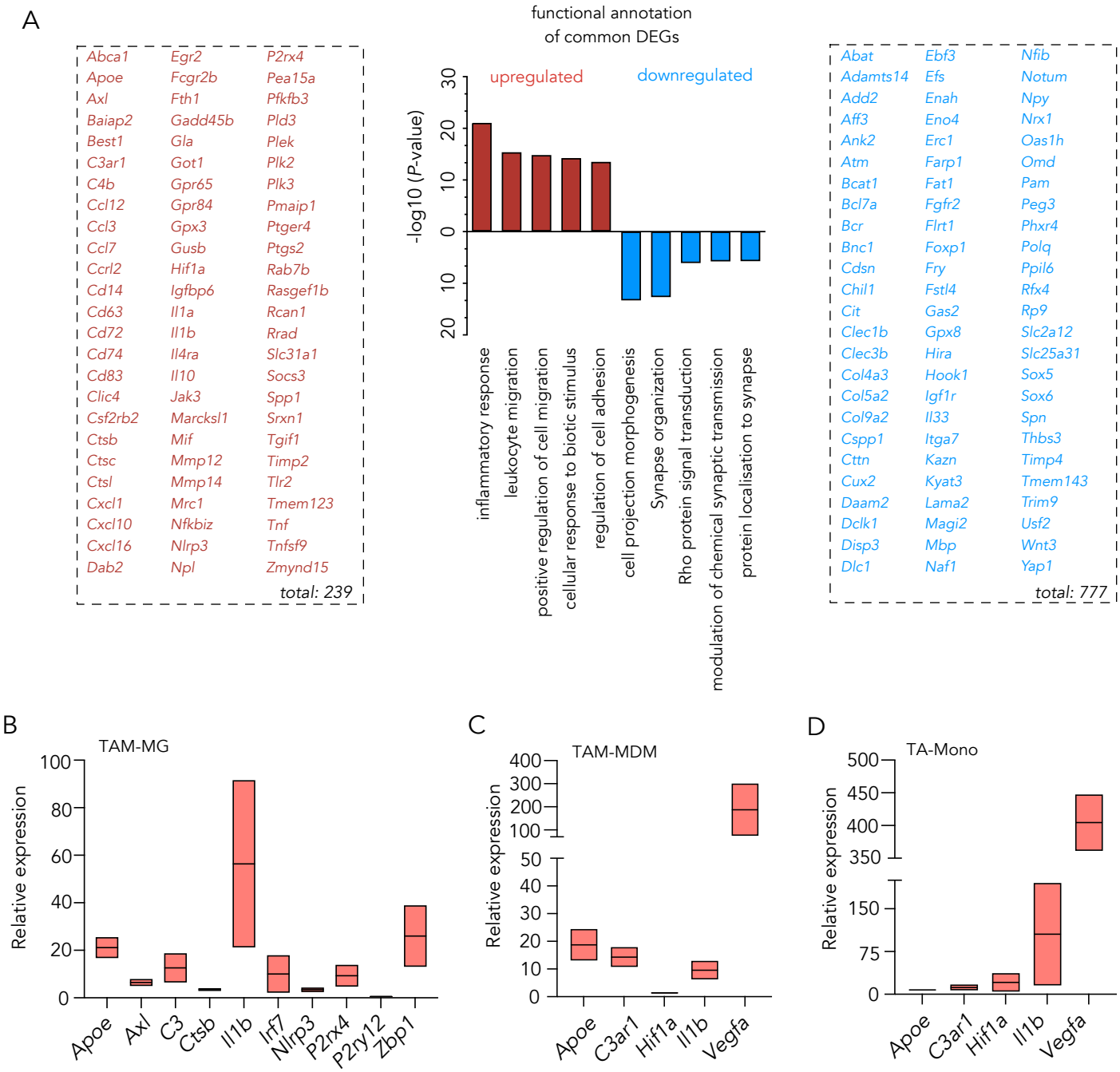

Figure S2. Tumor education signatures in TAMs, related to Figure 2. (A) Selected up- (red) or down (blue) regulated common genes in tumor-associated myeloid populations compared to normal controls and plot of the top 5 corresponding functional pathways. **(B-D)** Validation of candidate genes by qRT-PCR. Gene expression of selected genes that show differential expression in (A) TAM-MG relative to N-MG (B) TAM-MDM relative to N-Mono and (C) TA-Mono relative to N-Mono. n=2 for all conditions and analyzed genes apart from *Apoe* in TAM-Mono with n=1. Data are represented as mean of RQ values ± RQ min and max.

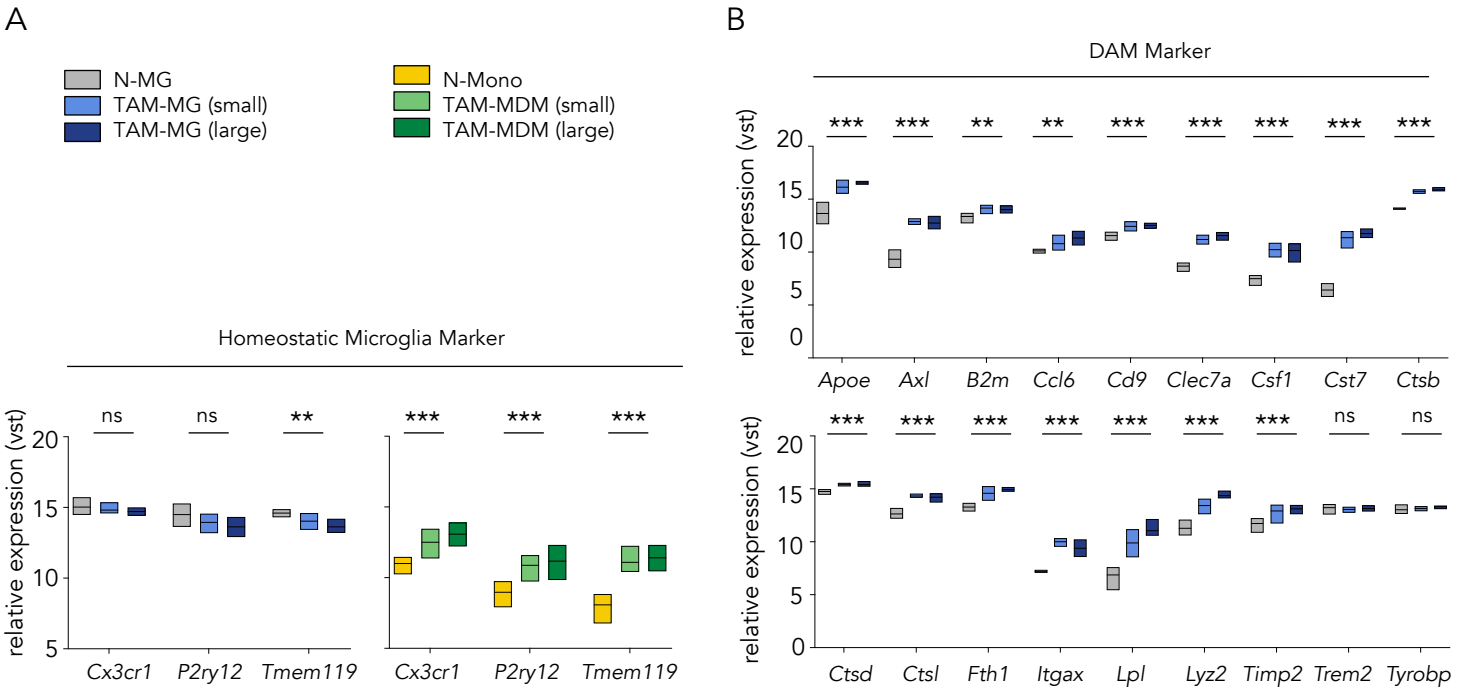

Figure S3. TAM-MG display similarities to DAMs, related to Figure 3. (A) Expression of homeostatic microglia marker in TAM-MG and TAM-MDM. **(B)** Expression of typical disease-associated microglia marker (derived from Keren-Shaul et al., 2017) in TAM-MG; for A and B: Values are derived from variance-stabilized data (vst (≈ log2)) of RNA-Seq data from the comparison control (N-MG or N-MONO, each n = 4) vs. TAM-MG/TAM-MDM (each in total n = 10). Significance based on padj values, with *P<0.05, **P<0.01 and ***P<0.001, ns = not significant.

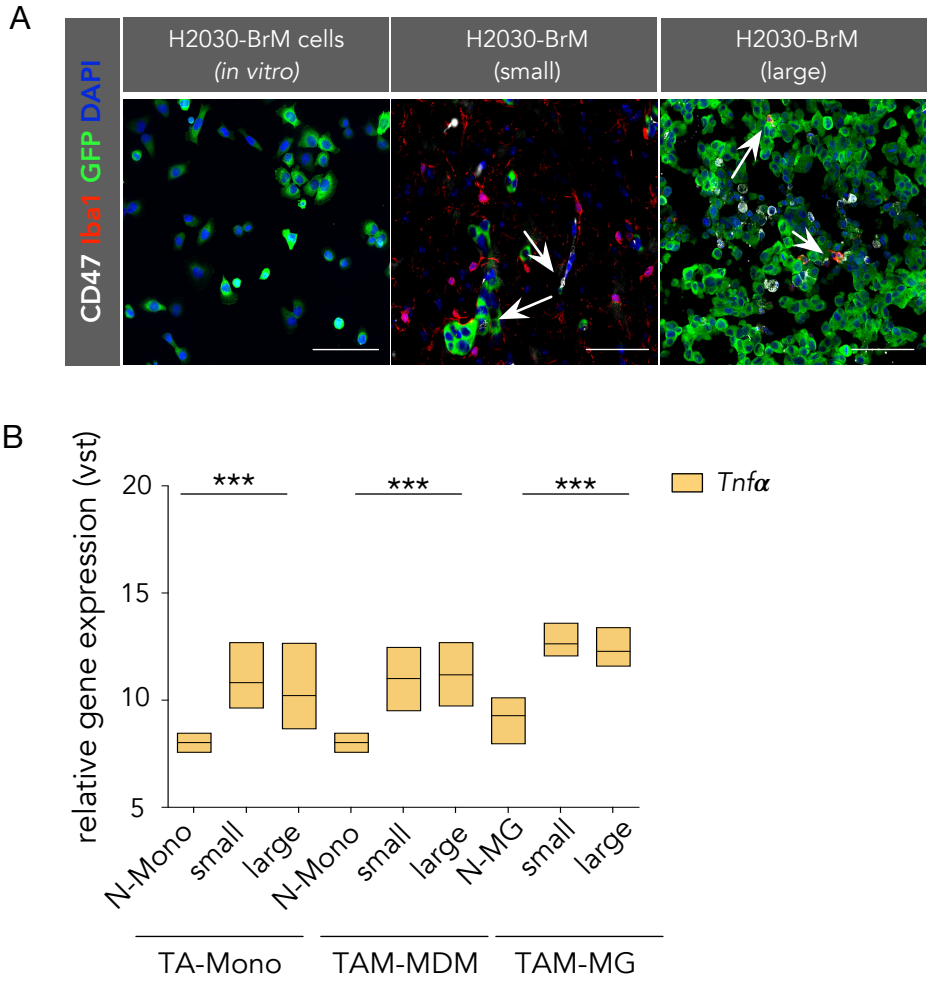

Figure S4. H2030 Tumor cells upregulate CD47 in vicinity to Iba1 positive cells, related to Figure 3. (A) Representative immunofluorescence images of H2030-BrM *in vitro* and H2030-BrM lesions *in vivo* stained for Iba1 (white) to visualize microglia/macrophages and CD47 (red). Tumor cells are stained for GFP (green). Arrows indicate CD47+ tumor cells in close vicinity to Iba1+ TAMs. Scale bar depicts 50 µm. **(B)** Quantification of relative expression levels of *Tnf* in comparison to CTRL cells (N-MG or N-Mono) vs. BrM-associated cells (small and large) (TA-Mono, TAM-MDMs, or TAM-MGs) based on values of variance-stabilized data (vst (≈ log2)) of RNA-Seq data. N-Mono: n=4, N-MG: n=4, small BrM-associated TA-Mono: n=4, all other groups: n=5. P values are based on padj, ***P<0.001

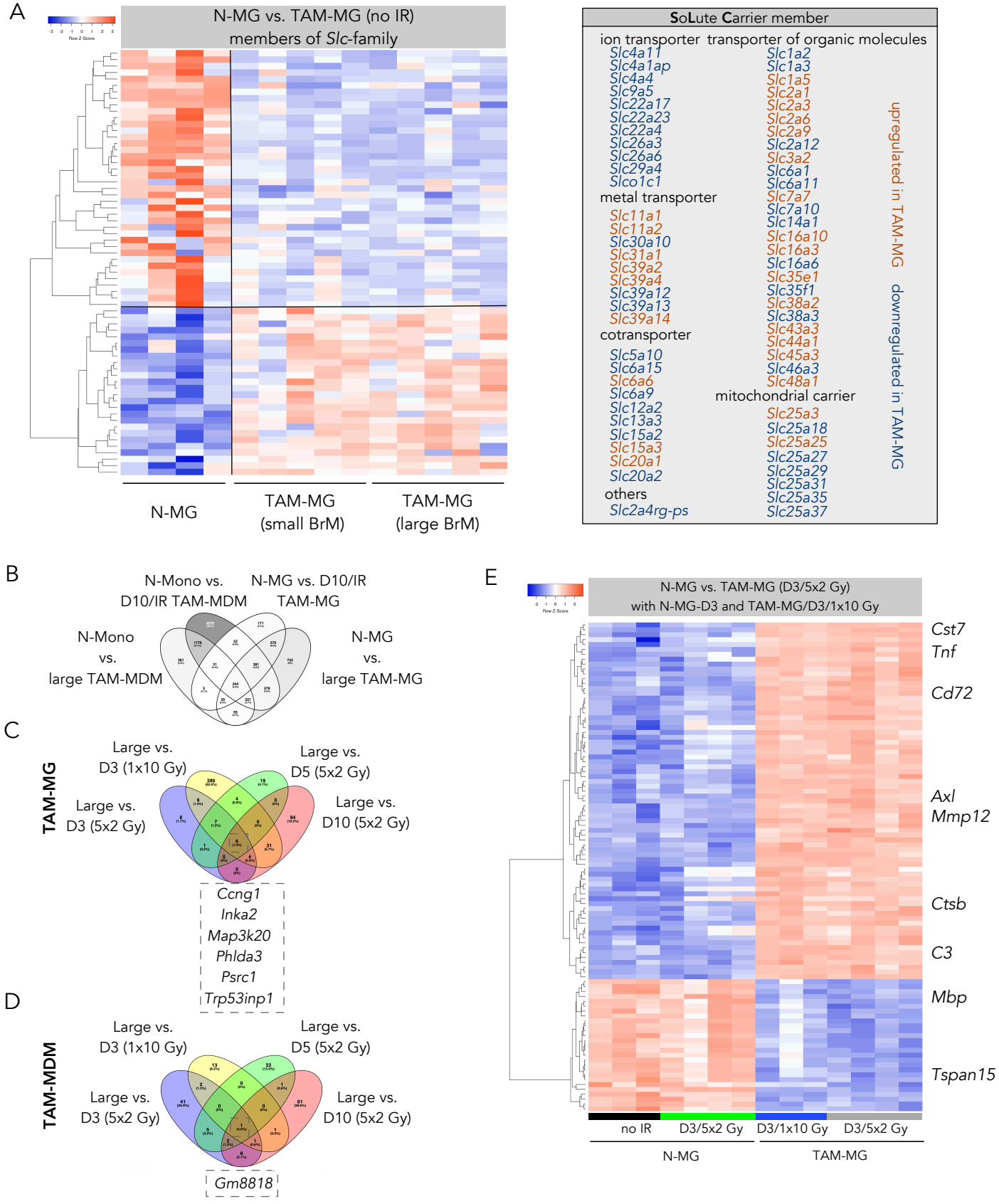

Figure S5. Transcriptomic profiles of irradiated TAM-MG and TAM-MDM, related to Figure 5. (A) Heatmap (left) and list (right) of the 66 differentially expressed "*Slc*"-family members in N-MG (n=4) vs. TAM-MG (small and large stage BrM, n=5 for each condition), cutoff: BM >20, adj. p<0.05. **(B)** Venn diagram displaying the number of DEGs (cutoff: BM >20) of RNA-Seq data comparisons between controls (N-Mono or N-MG, n=4) with either large stage TAM-MDM or TAM-MGs (n=5), or samples ten days after WBRT (n=3). **(C-D)** Venn diagrams of (C) TAM-MG and (D) TAM-MDM. Comparison of RNA-Seq data of large stage (n=5) BrM samples vs. WBRT (5x2 Gy/d3 and d5 n=4, 1x10 Gy/d3 and 5x2 Gy/d10 n=3). **(E)** Unsupervised hierarchical clustering heatmap depicting the Top 100 DEGs in N-MG vs. TAM-MG/D3 (5x2 Gy) including irradiated N-MG at d3 upon 5x2 Gy, as well as TAM-MG at d3 upon 1x10 Gy WBRT.

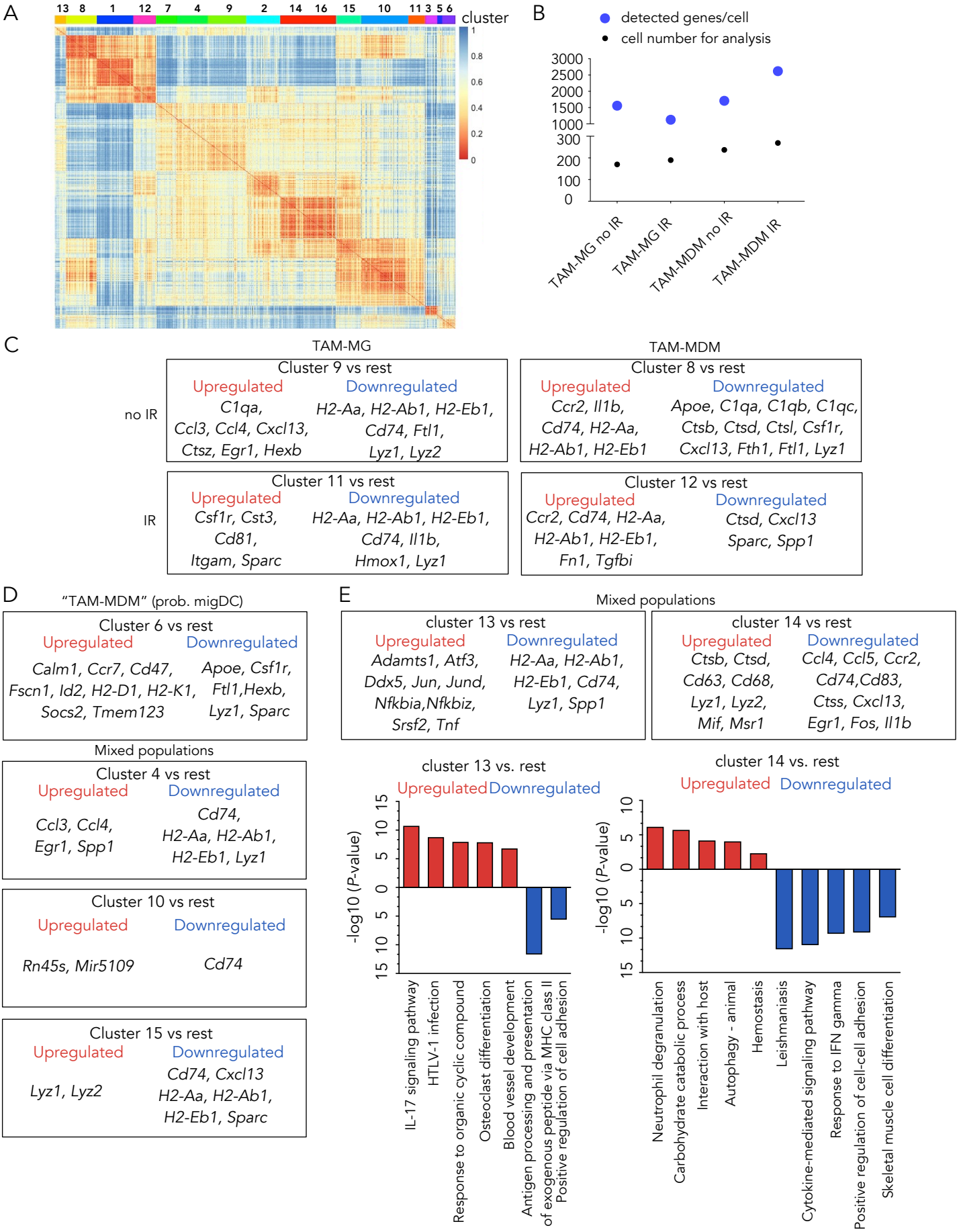

Figure S6. Single cell RNAseq reveals heterogeneous TAM populations, related to Figure 6. (A) Correlation plot depicting clustering of the analyzed cells of each experimental condition **(B)** Number of mean detected genes per cell and the cell number used for analysis. across all experimental groups. **(C-E)** List of up- and downregulated marker genes for indicated clusters, with corresponding functional gene annotation for cluster 13 and 14 (E), with up- (red) and downregulated (blue) genes for selected clusters. A maximum of five pathways is represented.

Table S3. List of antibodies, Related to Figure 1, Figure 3, Figure 4, Figure S1, Figure S4

Antibodies used for histology

Antigen	Host	Clonality / Clone	Dilution	Vendor	Cat No
C1q	rat	monoclonal / 7H8	1:100	abcam	ab11861
C3/C3a	chicken	polyclonal	1:200	abcam	ab48581
C3ar1	rat	monoclonal / 14D4	1:1,000	Hycult Biotech	HM1123
CD47	rat	monoclonal / miap301	1:200	Thermo Fisher Scientific	50-126-11
Collagen-IV	rabbit	polyclonal	1:200	Merck	AB756P
Factor H	sheep	polyclonal	1:500	abcam	Ab8842
Gfap	goat	polyclonal	1:1,000	abcam	ab53554
GFP	chicken	polyclonal	1:1,000	abcam	ab13970
Iba1	rabbit	polyclonal	1:1,000	Wako Chemicals	019-19741
Ki67	rat	monoclonal / SolA15	1:500	Thermo Fisher Scientific	50-245-563
Ly6G	rat	monoclonal / RB6-8C5	1:200	abcam	ab25377
NeuN	rabbit	monoclonal / EPR12763	1:10,000	abcam	ab177487
Tmem119	guinea pig	polyclonal	1:1,000	sysy	400004

Antibodies used for flow cytometry

Antigen	Host	Clone	Fluorochrome	Dilution	Vendor	Cat No
CD11b	rat	M1-70	BV605	1:1,000	BD	563015
CD45	rat	30-F11	A700	1:500	Biolegend	103128
CD49d	rat	R1-2	Pe-Cy7	1:500	Biolegend	103618
Ly6C	rat	HK1.4	PerCP-Cy5.5	1:250	Biolegend	128012
Ly6G	rat	1A8	BV421	1:500	BD	562737

TRANSPARENT METHODS

Mice

All animal studies were approved by the government committee (Regierungspräsidium Darmstadt, Germany) and were conducted in accordance with the requirements of the German Animal Welfare Act. Athymic/nude mice (CAnN.Cg-*Foxn1*^{nu}/Crl) were purchased from Charles River Laboratories or bred within the GSH animal facilities. Six to eight-week old females were used for experiments with brain metastatic mice and RNAseq analysis. For qRT-PCR validation female and male mice were used.

Cell lines

Brain metastatic (BrM) variants of the human lung cancer cell line H2030 (here denoted as H2030-BrM) were provided by Dr. Joan Massagué, MSKCC, and labeled with a triple-imaging vector (TK-GFP-Luc; TGL) to allow for non-invasive *in vivo* imaging of tumor growth over time. H2030-BrM cells were cultured in RPMI 1640 medium supplemented with 10 % FBS, 2mM L-Glutamine and 100 units/ml penicillin-streptomycin.

Secretome Analysis of H2030

Secreted factors present in H2030 supernatant were determined using a human multiplex cytokine assay (BioRad, Ca, USA) according to the manufacturer's instructions and analyzed on a Bioplex200 (BioRad). Complete RPMI media was used as reference control. The Bioplex-Manager software (v. 6.1) was used for acquisition of raw data. Data were obtained from three biological replicates.

Generation of experimental brain metastasis and *in vivo* BLI measurements

Generation of experimentally induced BrM was performed as previously described (Bos et al., 2009). Mice were anesthetized with ketamine / xylazine and $5x10^4$ cells in 100 µl 1x PBS were inoculated into the left ventricle of 6 to 8-week old Athy/nu mice (intra-cardiac injection = i.c.). Starting 3 weeks after i.c. injection, BrM progression was monitored weekly via bioluminescence imaging (BLI) (Caliper Life Sciences, Ivis Lumina II), following subcutaneous injection of 100 µl luciferin (15 mg/ml). Mice were anesthetized with isoflurane (2%) during the measurement. For

further experiments, animals were stratified into groups based on BLI-values (radiance = p/s/cm^2/sr) showing an BLI output range of 5x10^5 to 7.5x10^7 for small, or 1x10^8 to 5.3x10^8 photons x sec^{-1} for large BrM lesions, respectively.

RNA isolation, cDNA synthesis and quantitative real-time PCR

RNA from bulk sorted cell populations was isolated with Trizol LS, resuspended in DEPC-treated water, and 0.5 - 1 µg of RNA was used for cDNA synthesis. The following Taqman assays were used for qRT-PCR: *Axl* Mm00437221_m1, *Apoe* Mm01307193_g1, *C3* Mm01232779_m1, *C3ar1* Mm02620006_s1, *Ctsb* Mm01310506_m1, *Hif1a* Mm00468869_m1, *Il1b* Mm00434228_m1, *Irf7* Mm00516793_g1, *Nlrp3* Mm00840904_m1, *P2rx4* Mm00501787_m1, *P2ry12* Mm01950543_s1, *Vegfa* Mm00437306_m1, *Zbp1* Mm01247052_m1. Assays have been run in triplicate and expression was normalized to Ubiquitin C (*Ubc* Mm02525934_g1) for each sample.

Whole Brain Radiotherapy

For Whole Brain Radiotherapy, mice were stratified into different groups based on BLI output. Radiotherapy was applied on d0 with the Small Animal Radiation Research Platform (SARRP, X-Strahl Ltd, Camberley, UK) (Wong et al., 2008) as previously described (Chae et al., 2019). The SARRP is equipped with an on-board Cone Beam CT (CBCT) system for diagnostic imaging and radiation treatment planning. The integrated Muriplan software allows contouring, image-guided treatment design, dose calculation and application of radiation. Mice were anesthetized with isoflurane (2.5 %), stabilized in the prone position and imaged by performing a CBCT operating at 60 kV and 0.8 mA. CBCT images were next transferred to the Murislice software and individual isocenters were selected for radiotherapy. Irradiation was applied as WBRT as fractionated doses with 2 Gy on 5 consecutive days or with a single dose of 10 Gy using a 10x10 mm collimator as 1 arc operating at 220 kV and 13 mA with 5.2 cGy sec^{-1}.

Tissue preparation and immunostaining

Tissue for frozen histology was fixed in 4% PFA overnight and subsequently transferred into 30% sucrose until the tissue was fully equilibrated. Tissues were then embedded in OCT (Tissue-Tek) and 5 µm cryostat tissue sections were used for subsequent analyses. Hematoxylin and eosin (H&E) staining was performed on an automated staining device (Leica Autostainer XL) in the

histology core facility of the GSH. For immunofluorescence, frozen sections were thawed and dried at room temperature and rehydrated. For standard staining protocols, tissue sections were blocked in 3% BSA + 0.1% Triton-X100 in PBS for 1 h at room temperature, followed by incubation with primary antibodies in 1.5% BSA overnight at 4°C or 2 h at room temperature. Primary antibody information and dilutions are listed in Table S3. Fluorophor-conjugated secondary antibodies were used at a dilution of 1:500 in 1.5% BSA in PBS for 1h at room temperature. DAPI was used as nuclear counterstain.

For histology on thick tissue sections, PFA-fixed brain samples were sliced in 350 µm thick sections using a Vibratome VT1200S (Leica). Brain slices were cleared using the X-Clarity tissue clearing system (Logos Biosystem). Tissue clearing was performed at 0.6 A for 3 h using the X-Clarity electrophoretic tissue clearing solution. Afterwards, unspecific protein binding was blocked with 3% BSA in PBS containing 0.1% Triton-X100 followed by incubation with primary antibodies (Table S3) for 24 h at room temperature and fluorophor-conjugated secondary antibodies (Jackson ImmunoResearch) were used at a dilution of 1:500 in 1.5% BSA in PBS overnight at room temperature. DAPI was used as nuclear counterstain.

Microscopy and image analysis

Thin-section immunofluorescence stainings were imaged using a Zeiss Axio Imager. M2 Fluorescence Microscope (Zeiss, Germany) using a 10, 20, or 40x objective. Immunofluorescence staining on cleared thick sections was visualized using the Yokogawa CQ1 confocal microscope (Yokogawa, Musashino, Japan) using a 10, or 20x objective.

Flow cytometry and fluorescence activated cell sorting (FACS)

For flow cytometry and cell sorting, mice were anesthetized with Ketamine/Xylazine. Blood was collected by cardiac puncture and animals were transcardially perfused with PBS. Brain metastases were macrodissected based on *ex vivo* BLI signal and dissociated using the Brain Tumor Dissociation Kit (Miltenyi). A single cell suspension was generated using the gentleMACS Octo dissociator. For non-tumor bearing controls, whole brain samples were dissociated. Cell suspensions were filtered through a 70 µm mesh filter followed by red blood cell lysis. Normal brain and brain metastases samples were incubated with Myelin Removal Beads (Miltenyi). Cell

suspensions were incubated for 5-10 min at 4°C with FC block followed by incubation with directly conjugated antibodies panels as well as eFluor-780 (live/dead-discrimination) for 15 min at 4°C. Antibodies for the flow panel can be found in the Table S3. All flow cytometry analyses were performed on a BD Fortessa device and FACS sorting was performed on a BD FACS Aria Fusion. Cells were sorted into 100 µl cold PBS. Samples were kept on ice until Trizol LS was added. Samples were frozen at -80°C for analyses of bulk populations. For single cell RNAseq, cells were sorted into pre-labelled 384 well plates and snap frozen on dry ice. Plates were stored at -80°C until further processing.

RNA sequencing, gene expression analysis and data presentation

RNA was isolated by chloroform extraction and isopropanol precipitation using a glycogen carrier. RNA-sequencing libraries were generated with the SMART-Seq preparation kit (CloneTech) and fragmented with the Nextera XT kit (illumina). Paired end, 150 base pair, sequencing was performed with an Illumina HiSeq2500. All steps were performed by Genewiz (New Jersey, USA). The following steps were performed as previously described (Michels et al., 2019). Pre-processing of fastq-files of bulk sequenced samples including filtering for quality scores, poly-A trimming, removal of N containing reads, artifact removal and clearing of rRNA contamination was achieved using a pipeline in the HUSAR platform, provided by DKFZ (Heidelberg, Germany). Transcriptomes were mapped to the mouse genome using the genecode annotations (release M12) and TopHat2 (v. 2.0.14) (Kim et al., 2013). The number of reads per gene was determined by HTSeq count. Overlaps were considered as unique. Further analysis was performed within R (v. 3.4.3), operating in RStudio (v. 1.1.453) with BioMart package (v. 2.34.1) and DESeq2 (v. 1.18.1) (Love et al., 2014). If not indicated otherwise, data for heatmaps and PCA-clustering were generated of variance-stabilized transformed data (which equals log2 transformation), respecting a BaseMean >20 and an adjusted p-value of 0.05 (= FDR 5 %). Data shown consist of 3 to 5 biological replicates per condition.

Original Euler plots were created with eulerr (v. 6.0.0). Venn-diagrams of selected data were created with Venny (v. 2.1; www.bioinfogp.cnb.csic.es/tools/venny/index.html) (Oliveros, 2015), and functional annotation of selected (top-) genes was done using *Metascape* (www.metascape.org) (Zhou et al., 2019). Un-/ and semi-supervised clustering and generation of

heatmaps was performed via manual selection of significant DEGs (base-mean >20 and padj <0.05 unless indicated otherwise), or TOP-X DEGs of variance- stabilized data. Heatmaps were processed in Heatmapper (http://www1.heatmapper.ca/expression) (Babicki et al., 2016) with default parameters, including *Complete Linkage Clustering* and *Spearman Rank Correlation* for distance measurement.

Single Cell RNAseq

RNA isolation, processing, reverse transcription, library preparation, and sequencing were performed based on the SORT-Seq protocol as previously described (Muraro et al., 2016). Quality control and data analysis was done with RaceID (Grun et al., 2016). Single cell RNA sequencing, quality control, raw data processing and analysis was performed by Single Cell Discoveries (SCD, Utrecht, Netherlands). Downstream analysis contained Poisson-corrected, UMI corrected raw mapped reads. For any further analysis, cells with an UMI >800 were used.

Quantification and statistical analysis

Summary data are presented as mean ± standard deviation, floating bars with lines indicating min, max and median or Tukey's box plots using GraphPad Prism software v7. Numerical data was analyzed using the statistical tests noted with the corresponding sections of the manuscript. Statistical analyses were performed with GraphPad Prism software v7 and R (version 3.4.3) performing tests as indicated and were considered statistically significant, with *P<0.05, **P<0.01 and ***P<0.001.

SUPPLEMENTAL REFERENCES

Babicki, S., Arndt, D., Marcu, A., Liang, Y., Grant, J. R., Maciejewski, A., and Wishart, D. S. (2016). Heatmapper: web-enabled heat mapping for all. Nucleic Acids Res *44*, W147-153.

Bos, P. D., Zhang, X. H., Nadal, C., Shu, W., Gomis, R. R., Nguyen, D. X., Minn, A. J., van de Vijver, M. J., Gerald, W. L., Foekens, J. A., and Massague, J. (2009). Genes that mediate breast cancer metastasis to the brain. Nature *459*, 1005-1009.

Chae, W. H., Niesel, K., Schulz, M., Klemm, F., Joyce, J. A., Prummer, M., Brill, B., Bergs, J., Rodel, F., Pilatus, U., and Sevenich, L. (2019). Evaluating Magnetic Resonance Spectroscopy as a

Tool for Monitoring Therapeutic Response of Whole Brain Radiotherapy in a Mouse Model for Breast-to-Brain Metastasis. Front Oncol *9*, 1324.

Grun, D., Muraro, M. J., Boisset, J. C., Wiebrands, K., Lyubimova, A., Dharmadhikari, G., van den Born, M., van Es, J., Jansen, E., Clevers, H., *et al.* (2016). De Novo Prediction of Stem Cell Identity using Single-Cell Transcriptome Data. Cell Stem Cell *19*, 266-277.

Kim, D., Pertea, G., Trapnell, C., Pimentel, H., Kelley, R., and Salzberg, S. L. (2013). TopHat2: accurate alignment of transcriptomes in the presence of insertions, deletions and gene fusions. Genome Biol *14*, R36.

Love, M. I., Huber, W., and Anders, S. (2014). Moderated estimation of fold change and dispersion for RNA-seq data with DESeq2. Genome Biol *15*, 550.

Michels, B. E., Mosa, M. H., Grebbin, B. M., Yepes, D., Darvishi, T., Hausmann, J., Urlaub, H., Zeuzem, S., Kvasnicka, H. M., Oellerich, T., and Farin, H. F. (2019). Human colon organoids reveal distinct physiologic and oncogenic Wnt responses. J Exp Med *216*, 704-720.

Muraro, M. J., Dharmadhikari, G., Grun, D., Groen, N., Dielen, T., Jansen, E., van Gurp, L., Engelse, M. A., Carlotti, F., de Koning, E. J., and van Oudenaarden, A. (2016). A Single-Cell Transcriptome Atlas of the Human Pancreas. Cell Syst *3*, 385-394 e383.

Oliveros, J. C. (2015). Venny. An interactive tool for comparing lists with Venn diagrams.

Wong, J., Armour, E., Kazanzides, P., Iordachita, I., Tryggestad, E., Deng, H., Matinfar, M., Kennedy, C., Liu, Z., Chan, T., *et al.* (2008). High-resolution, small animal radiation research platform with x-ray tomographic guidance capabilities. Int J Radiat Oncol Biol Phys *71*, 1591-1599.

Zhou, Y., Zhou, B., Pache, L., Chang, M., Khodabakhshi, A. H., Tanaseichuk, O., Benner, C., and Chanda, S. K. (2019). Metascape provides a biologist-oriented resource for the analysis of systems-level datasets. Nat Commun *10*, 1523.